

## Permeability enhancement and void formation by chelating agent in volcanic rocks (Ahuachapán and Berlín geothermal fields, El Salvador)

Luis Salalá<sup>a,b</sup>, Ryota Takahashi<sup>a</sup>, Jonathan Argueta<sup>a,c</sup>, Jiajie Wang<sup>a</sup>, Noriaki Watanabe<sup>a,\*</sup>, Noriyoshi Tsuchiya<sup>a</sup>

<sup>a</sup> Department of Environmental Studies for Advanced Society, Graduate School of Environmental Studies, Tohoku University, Sendai 980-8579, Japan

<sup>b</sup> Department of Mechanical Engineering, Faculty of Engineering and Architecture, University of El Salvador, San Salvador, El Salvador

<sup>c</sup> Department of Graduate Studies, Faculty of Engineering and Architecture, University of El Salvador, San Salvador, El Salvador

### ARTICLE INFO

#### Keywords:

Chelating agent  
Chemical stimulation  
Enhanced geothermal system  
Geothermal energy  
Induced seismicity  
Permeability enhancement

### ABSTRACT

Chemical stimulation using environment-friendly chelating agents (e.g., readily biodegradable GLDA) was recently shown to rapidly and substantially enhance the permeability of fractured granite, without creating mineral precipitation. This study examined the effectiveness of such stimulation in volcanic rocks through flooding experiments conducted with a pH 4 GLDA solution on fractured dacitic, andesitic, and basaltic rocks from geothermal fields in El Salvador at 200 °C under confining pressure. Results showed substantial permeability enhancement of up to 4.3-fold in 2 h, where the magnitude of enhancement depended mainly on the initial proportion of Fe-rich phenocrysts, which dissolved to form voids.

### 1. Introduction

In recent years, enhanced geothermal systems (EGSs) have been developed to enable or increase power generation from geothermal reservoirs with high temperatures but low initial permeabilities (Breede et al., 2013; Massachusetts Institute of Technology, 2006). Creating EGSs involves increasing the permeability of such geothermal reservoirs through hydraulic, thermal, and/or chemical stimulation (Cladouhos et al., 2016; Farquharson et al., 2020; Lucas et al., 2020; Luo et al., 2018; McClure and Horne, 2014; Park et al., 2017; Portier et al., 2009; Sirtovich et al., 2011). Hydraulic stimulation, a procedure in which high-pressure fluid leads to shear dilation of pre-existing fractures and/or the creation of new ones, is the most widely used and studied among these methods. However, the potential for hydraulic stimulation to trigger seismic activity is concerning (Deichmann and Giardini, 2009; Grigoli et al., 2018; Kim et al., 2018b,a; Zang et al., 2014). This method must be used carefully in conjunction with injection flow rates and pressures of moderate intensities (Kim et al., 2018b; Kwiatek et al., 2019). Reduction of intensity will lead to an insufficient enhancement of permeability. If the permeability is not sufficiently improved, subsequent longer injections at higher pressures and/or longer injection times can be used to induce larger slips in initially large or coalesced fractures (Watanabe et al., 2008; Nemoto et al., 2009; Watanabe et al., 2009;

Ishibashi et al., 2015, 2016), but such additional injections can increase the risk of induced seismicity. Therefore, chemical stimulation may be necessary to balance the competing concerns of inadequate permeability enhancement and induced seismicity from hydraulic stimulation.

Chemical stimulation entails the injection of acid into a reservoir to dissolve hydrothermal minerals precipitated in fractures near the wellbore, or to create larger-aperture fractures via mineral dissolution rather than shear dilation (Farquharson et al., 2020; Lucas et al., 2020; Luo et al., 2018; Portier et al., 2009). However, conventional chemical stimulation uses hydrochloric and hydrofluoric acids and is known to be less efficient in dissolving minerals over long distances. Additionally, because such strong mineral acids are highly reactive and because fluid chemistry is highly variable in space and time, it is extremely difficult to predict all possible dissolution and precipitation reactions and their impacts on permeability.

To overcome these disadvantages of conventional strong mineral acids, a recent study (Watanabe et al., 2021) proposed the use of chelating agents to selectively dissolve rock-forming minerals in geothermal environments and to enhance rock fracture permeability. Among the various types of chelating agents, environmentally friendly compounds, such as N-(2-hydroxyethyl)ethylenediamine-N, N', N'-tri-acetic acid (HEDTA) and readily biodegradable N, N-bis(carboxymethyl)-L-glutamic acid (GLDA), were found to be suitable for use in

\* Corresponding author.

E-mail address: [noriaki.watanabe.e6@tohoku.ac.jp](mailto:noriaki.watanabe.e6@tohoku.ac.jp) (N. Watanabe).

natural environments (Mahmoud et al., 2017; Pinto et al., 2014; Wang et al., 2021, 2022). Even in weakly acidic aqueous solutions, minerals have high dissolution rates due to the combined effects of the chelating agent and hydrogen ions (Fredd and Fogler, 1998). Mineral dissolution is accelerated through chelating agents, and metal ions are stabilized through chelation over longer distances. Moreover, the degree to which the dissolution rate is enhanced varies with the type of mineral. Consequently, the selective dissolution of rock-forming minerals can be achieved, creating voids, within a framework of less soluble minerals, that remain open under confining stress at depth.

In a previous study (Watanabe et al., 2021), chelating agent flooding experiments were conducted on fractured granite under confining stress at 200 °C, using 20 wt% aqueous solutions of sodium salts of HEDTA and GLDA at pH 4. These resulted in a rapid and substantial enhancement in permeability, accompanied by void formation due to the selective dissolution of biotite (i.e., Fe-rich mineral). However, such permeability enhancement due to selective mineral dissolution has neither been demonstrated nor investigated in fractured, non-crystalline volcanic rocks, which comprise the bulk of currently or potentially exploitable geothermal resources around the world. This new method of chemical stimulation is expected to be effective even in volcanic rocks containing phenocrysts of Fe-rich minerals, such as biotite, hornblende, pyroxenes, and olivine.

Therefore, in the present study, we examined the effectiveness of chelating-agent-based chemical stimulation on fractured volcanic rocks, by conducting chelating agent flooding experiments on core samples of different volcanic rocks obtained from geothermal fields in El Salvador. The experiments were conducted under confining stress at 200 °C using a 20 wt% aqueous solution of sodium salt of GLDA at a pH of 4.

## 2. Materials and methods

### 2.1. Fractured volcanic rock samples and chelating agent

Three cylindrical samples (diameter: 25 mm, length: 25 mm) were prepared from dacitic, andesitic, and basaltic rocks (Samples A, B, and C, respectively) obtained from the Ahuachapán and Berlín geothermal fields, El Salvador (Fig. 1). Each sample contained a tensile fracture parallel to the sample axis (i.e., macroscopic flow direction in the flooding experiment), which was induced by the Brazilian test.

Quantitative elemental analysis using an electron probe micro-analyzer (EPMA; JEOL JXA-8200) was conducted on thin sections from the three types of volcanic rocks to determine their chemical compositions and mineral distributions. The Total Alkali-Silica (TAS) classification system was used to classify the samples, based on their major element compositions (Table 1). The rocks used to prepare Samples A, B, and C were identified as dacitic, andesitic, and basaltic rocks, respectively, as stated above. Among the elements listed in Table 1, elution of Ti, Al, Fe, Mg, Ca, and Mn from the rock into water could be accelerated by the presence of a chelating agent.

Samples A and B contained plagioclase, orthopyroxene,



Fig. 1. Three types of volcanic rocks used in the chelating agent flooding experiments: Sample A, Sample B, and Sample C were prepared from dacitic, andesitic, and basaltic rocks, respectively.

Table 1

Representative element concentrations (wt%; EPMA analyses) for each rock sample.

	Sample A	Sample B	Sample C
SiO <sub>2</sub>	63.7	57.0	50.8
TiO <sub>2</sub>	0.6	0.8	1.2
Al <sub>2</sub> O <sub>3</sub>	15.9	17.5	16.7
FeO	4.6	7.3	11.3
MgO	1.2	2.4	3.4
CaO	3.4	6.6	7.9
Na <sub>2</sub> O	4.9	3.7	3.6
K <sub>2</sub> O	2.7	1.5	1.2
P <sub>2</sub> O <sub>5</sub>	0.2	0.1	0.4
MnO	0.1	0.1	0.2
Total	97.3	97.1	96.8

clinopyroxene, and hematite as phenocrysts (grain size:  $\geq 0.1$  mm) within a silica-rich groundmass, while Sample C contained plagioclase, clinopyroxene, hematite, and olivine as phenocrysts within a similarly silica-rich groundmass (Table 2). The areal percentage and average size of the phenocrysts contained in the thin-section of each sample are summarized in Table 3. Among the phenocrysts, Fe-rich minerals (i.e., all those mentioned except for plagioclase) were expected to dissolve in the flooding experiments, as selective dissolution of Fe-rich biotite was observed in the previous flooding experiments conducted on fractured granite (Watanabe et al., 2021). The total areal percentage of the Fe-rich phenocrysts was 2.1% for Sample A, 19.7% for Sample B, and 0.6% for Sample C, and the average size of such phenocrysts was similar (approximately 0.2 mm) for all samples. Consequently, the degree of permeability enhancement was expected to be larger for Sample B, followed by those for Sample A and Sample C.

Aqueous solutions containing GLDA were prepared from approximately 40 wt% aqueous solution of GLDA-Na<sub>4</sub> (C<sub>9</sub>H<sub>9</sub>NNa<sub>4</sub>O<sub>8</sub>), purchased from Tokyo Chemical Industry Co., Ltd. (Tokyo, Japan). These solutions contained GLDA-Na<sub>4</sub> at approximately 20 wt% and were adjusted to pH values of 4 with nitric acid (HNO<sub>3</sub>, 60–61%, Kanto Chemical, Japan).

### 2.2. Experimental system, procedures, and conditions

The experimental system and procedures described in this section are the same as those in our previous study (Watanabe et al., 2021). The chelating agent flooding experiments were conducted using the experimental system shown in Fig. 2. In each trial, a Viton-sleeved sample with end-plugs attached to both inlet and outlet faces was placed horizontally in a pressure vessel maintained at 200 °C using a mantle heater. Silicone oil was pumped into the vessel at a constant pressure to subject the sample to a confining pressure of 15 MPa, representing the confining stress in geothermal environments. The initial permeability of the sample was determined based on Darcy's law, by first pumping pure water into the sample at a constant flow rate of either 0.25 or 1.00 mL min<sup>-1</sup>, depending on the initial flow resistance of the sample. More specifically, a flow rate of 0.25 mL min<sup>-1</sup> was maintained for Sample A, while a flow rate of 1.00 mL min<sup>-1</sup> was used for the other two samples. The permeability ( $k$ ) was then calculated according to Darcy's law as follows:

$$k = \frac{Q\mu L}{\pi r^2 \Delta P} \quad (1)$$

where  $Q$  is the flow rate;  $\mu$  is the viscosity of the injected fluid;  $\Delta P$  is the differential pressure of the fluid between the inlet and outlet faces of the sample; and  $r$  and  $L$  are the radius and length of the sample, respectively. During this process, the water flowed out of the sample through a backpressure regulator adjusted to 5 MPa. After determining the initial permeability, the aqueous chelating agent solution was injected into the sample at the same flow rate for 2 h. Effluent samples were collected at

**Table 2**

Element concentrations (wt%; EPMA analyses) of phenocrysts and groundmass in each sample, where Pl, Cpx, Opx, Hem, Ol, and Gnd, respectively, denote plagioclase, clinopyroxene, orthopyroxene, hematite, olivine, and groundmass.

Phenocryst/Groundmass	Sample A					Sample B					Sample C				
	Pl	Cpx	Opx	Hem	Gnd	Pl	Cpx	Opx	Hem	Gnd	Pl	Cpx	Opx	Hem	Gnd
SiO <sub>2</sub>	50.2	52.3	52.1	0.2	77.6	55.7	51.5	52.4	0.2	80.4	47.6	50.6	36.8	0.1	74.5
TiO <sub>2</sub>	0.1	0.4	0.2	14.7	0.4	0.0	0.3	0.2	5.9	0.4	0.0	0.8	0.0	11.0	0.3
Al <sub>2</sub> O <sub>3</sub>	28.9	1.3	1.6	2.0	11.4	26.2	1.5	0.8	2.8	9.1	30.3	2.0	0.1	3.8	9.5
FeO	0.5	10.4	20.1	76.0	2.2	0.5	10.6	21.0	83.0	1.7	0.8	15.5	28.6	76.0	2.9
MgO	0.1	14.4	18.6	1.6	0.3	0.0	11.7	18.7	0.5	0.5	0.0	12.6	27.8	1.9	1.4
CaO	15.5	20.4	1.5	0.0	0.3	10.8	22.0	1.6	0.0	0.9	16.7	17.4	0.2	0.0	3.8
Na <sub>2</sub> O	3.2	0.3	0.1	0.3	2.6	6.2	0.4	0.0	0.0	2.0	2.7	0.3	0.0	0.0	2.1
K <sub>2</sub> O	0.1	0.0	0.0	0.0	4.0	0.3	0.0	0.0	0.0	3.2	0.1	0.1	0.0	0.0	3.7
MnO	0.1	0.5	0.8	0.6	0.1	0.0	0.6	0.8	0.1	0.0	0.0	0.5	0.6	0.3	0.1
Total	98.6	100.0	95.1	95.5	98.9	99.8	98.6	95.3	92.5	98.1	98.2	99.8	94.1	93.1	98.3

**Table 3**

Areal percentage and average size of phenocrysts in each sample, where Pl, Cpx, Opx, Hem, Ol, and Gnd, respectively, denote plagioclase, clinopyroxene, orthopyroxene, hematite, olivine, and groundmass.

	Pl		Cpx		Opx		Hem		Ol	
	Areal pct. (%)	Avg. size (mm)								
Sample A	12.2	0.195	0.8	0.173	0.8	0.173	0.5	0.186	–	–
Sample B	29.5	0.235	6.9	0.225	10.9	0.256	1.9	0.198	–	–
Sample C	15.4	0.147	0.4	0.265	–	–	0.2	0.143	0.9	0.23

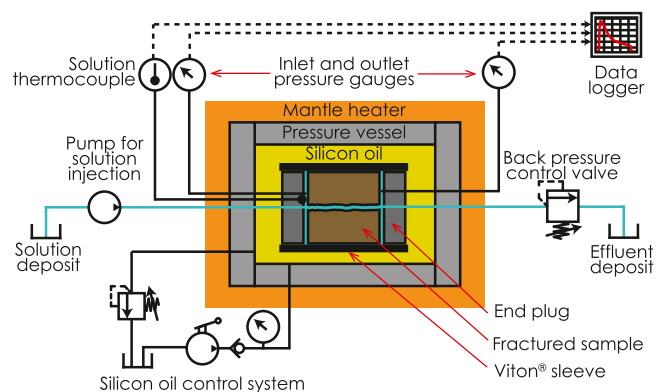


Fig. 2. Experimental system for chelating agent flooding experiments.

constant intervals of either 10 min (at 1.00 mL min<sup>-1</sup>) or 20 min (at 0.25 mL min<sup>-1</sup>) throughout each experiment. These aliquots were analyzed to determine the concentrations of Al, Ca, Fe, K, Mg, Si, and Ti using inductively coupled plasma optical emission spectrometry (ICP-OES, Agilent 5100).

X-ray computed tomography (CT) was conducted on each sample before and after the chelating agent flooding experiment, with a tube voltage of 120 kV, a tube current of 150  $\mu$ A, and a voxel size of 20  $\mu$ m  $\times$  20  $\mu$ m  $\times$  20  $\mu$ m. The Molcer Plus 3D image visualization and processing software (White Rabbit Corp., Tokyo, Japan) (Tanaka et al., 2013) was used to compute a distribution of significantly large pores and fracture apertures (i.e., voids) with sizes similar to or larger than the voxel size. Blender 3D (Blender Online Community, 2018) was used for visualization of 3D distribution of the voids.

### 3. Results and discussion

#### 3.1. Evolution of rock permeability and fluid chemistry

Fig. 3 shows the changes in differential pressure between the inlet and outlet of the sample as a function of time. The differential pressure is

a proxy of the hydraulic resistance based on Darcy's law, represented by Eq. (1). Therefore, permeability enhancement during injection of the GLDA solution corresponds to a decrease in the differential pressure. In all experiments, the differential pressure was almost constant during the water injection (time < 0 min in the figure) because of the insignificant water-rock reaction. In contrast, after injection of the GLDA solution had begun, the differential pressure first increased (because the GLDA solution is more viscous than water) and then decreased (due to enhanced permeability of the sample). The factor of permeability enhancement was defined as the ratio between the peak and final differential pressure values, as indicated by the red arrows in the figure. It should be noted that the sudden drop in differential pressure prior to injection of the GLDA solution was due to the pump being stopped when the fluid was switched from water to the chelating agent solution, because the same pump was used for both fluids (Fig. 2).

In all experiments, the differential pressure decreased (i.e., permeability increased) more rapidly during the early stage of the GLDA solution injection. Similar changes in the differential pressure were reported for the GLDA flooding experiments on fractured granite (Watanabe et al., 2021), in which voids were formed due to the selective dissolution of biotite (i.e., Fe-rich mineral with a low volumetric proportion of <10%). Therefore, the permeability enhancement in the present experiments was likely triggered by void formation due to selective dissolution of phenocrysts, rather than of fine-grained Fe-rich minerals (pyroxenes, hematite, and/or olivine) in the groundmass. The factor of permeability enhancement was 1.5-fold for Sample A, 4.3-fold for Sample B, and 1.2-fold for Sample C, where the initial permeability was  $7.97 \times 10^{-18}$  m<sup>2</sup> for Sample A,  $1.46 \times 10^{-16}$  m<sup>2</sup> for Sample B, and  $1.38 \times 10^{-15}$  m<sup>2</sup> for Sample C. These improvements occurred rapidly (within 2 h) and are significant because they are comparable to improvements in injectivity index obtained by conventional chemical stimulation in geothermal fields (Portier et al., 2009) as well as the permeability enhancement factors observed for the fractured granite in the GLDA flooding experiments (Watanabe et al., 2021). This demonstrates the effectiveness of chelating-agent-based chemical stimulation on fractured volcanic rocks. Additionally, as expected, a larger permeability enhancement was observed in the sample with a larger areal percentage of Fe-rich mineral phenocrysts. Notably, the decrease in

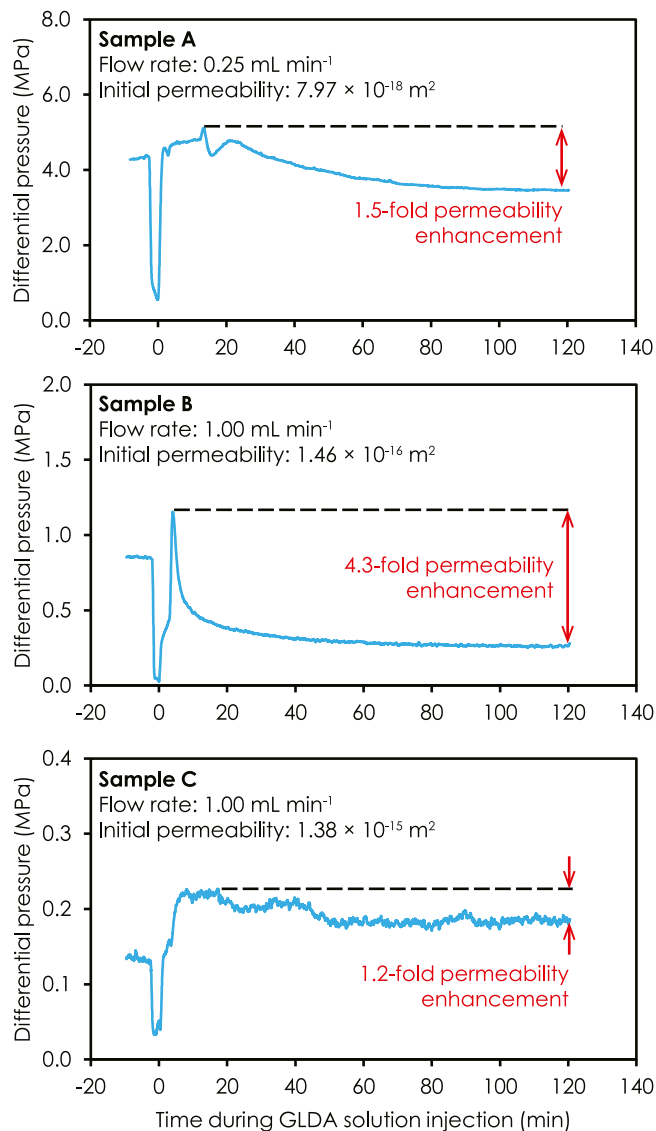


**Fig. 3.** Changes in differential pressure in the experiments on Samples A, B, and C. The factor of permeability enhancement is defined as the ratio between the peak and final differential pressure values, indicated by red arrows. (For interpretation of the references to color in this figure legend, the reader is referred to the web version of this article.)

differential pressure was less smooth in Sample C, implying competing processes of both permeability enhancement and reduction, as discussed in Section 3.2.

Fig. 4 shows the changes in the elemental concentrations and pH of the effluents as a function of time, wherein the concentration and pH at 0 min were obtained for the effluent before the GLDA solution was injected. The concentrations of all elements in the effluent increased significantly after the injection of the GLDA solution, reflecting enhanced dissolution of phenocrysts and/or groundmass in the sample. However, the rapid and remarkable increase in the concentration of Fe indicates void formation due to the selective dissolution of Fe-rich mineral phenocrysts (pyroxenes, hematite, and/or olivine). This interpretation is based on the void formation observed in a previous study, which occurred due to the selective dissolution of biotite in granite (Watanabe et al., 2021) and was accompanied by a similar change in Fe concentration. Although the GLDA solution may have accelerated the dissolution of all phenocrysts and groundmass, permeability enhancement seemed to be triggered by void formation due to the selective dissolution of phenocrysts of Fe-rich minerals, because the changes in

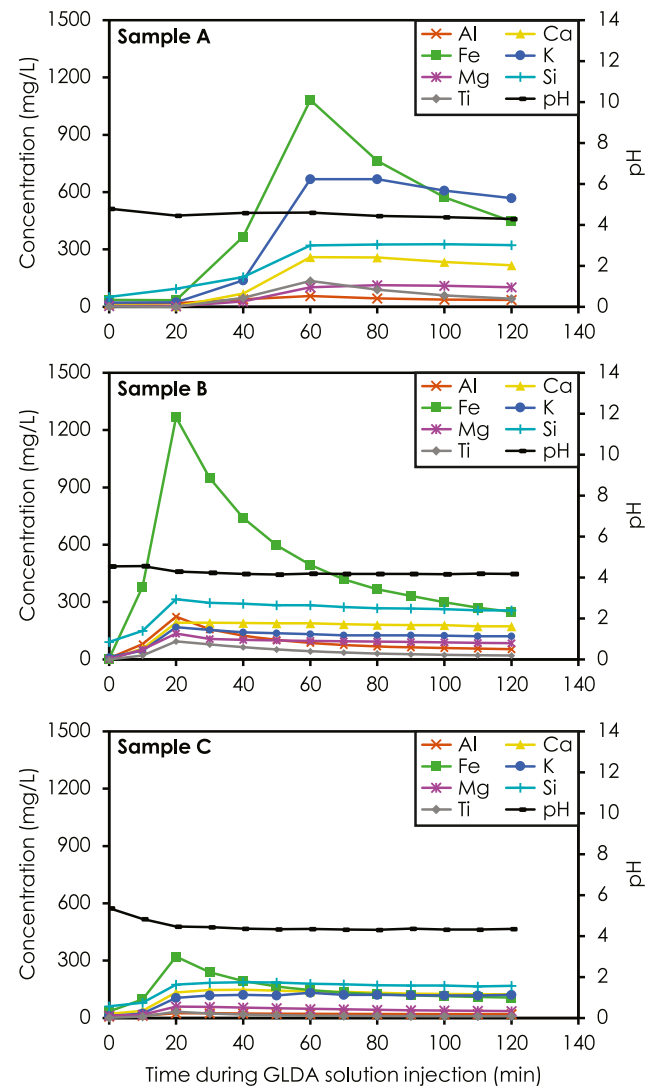


**Fig. 4.** Changes in elemental concentrations and pH during injection of the GLDA solution into Samples A, B, and C.

differential pressure were similar to the changes in Fe concentration.

### 3.2. Void formation by selective dissolution of Fe-rich minerals

Fig. 5 compares the selected X-ray CT slice images for each sample before and after the experiment to confirm void formation by selective dissolution of Fe-rich phenocrysts (pyroxenes, hematite, and/or olivine). It should be noted that these images were selected to compare very similar slices, although they may not precisely present the same slices. In all the images, plagioclase and groundmass appear as similar grey areas, and fractures and pores appear as darker grey or black areas. In Fig. 5, orthopyroxene and clinopyroxene are indicated by light blue (Samples A and B), clinopyroxene and olivine are indicated by green (Sample C), and hematite is indicated by red (all samples). It should be noted that the large pores (voids) initially contained in Sample B had limited connectivity and thus did not contribute significantly to permeability.

The X-ray CT slice images of Samples A and B clearly demonstrate the formation of voids through selective dissolution of pyroxene and hematite phenocrysts along the fracture plane. In contrast, the images of Sample C revealed a widened fracture aperture due to selective dissolution along the fracture plane. Clinopyroxene and/or olivine (likely

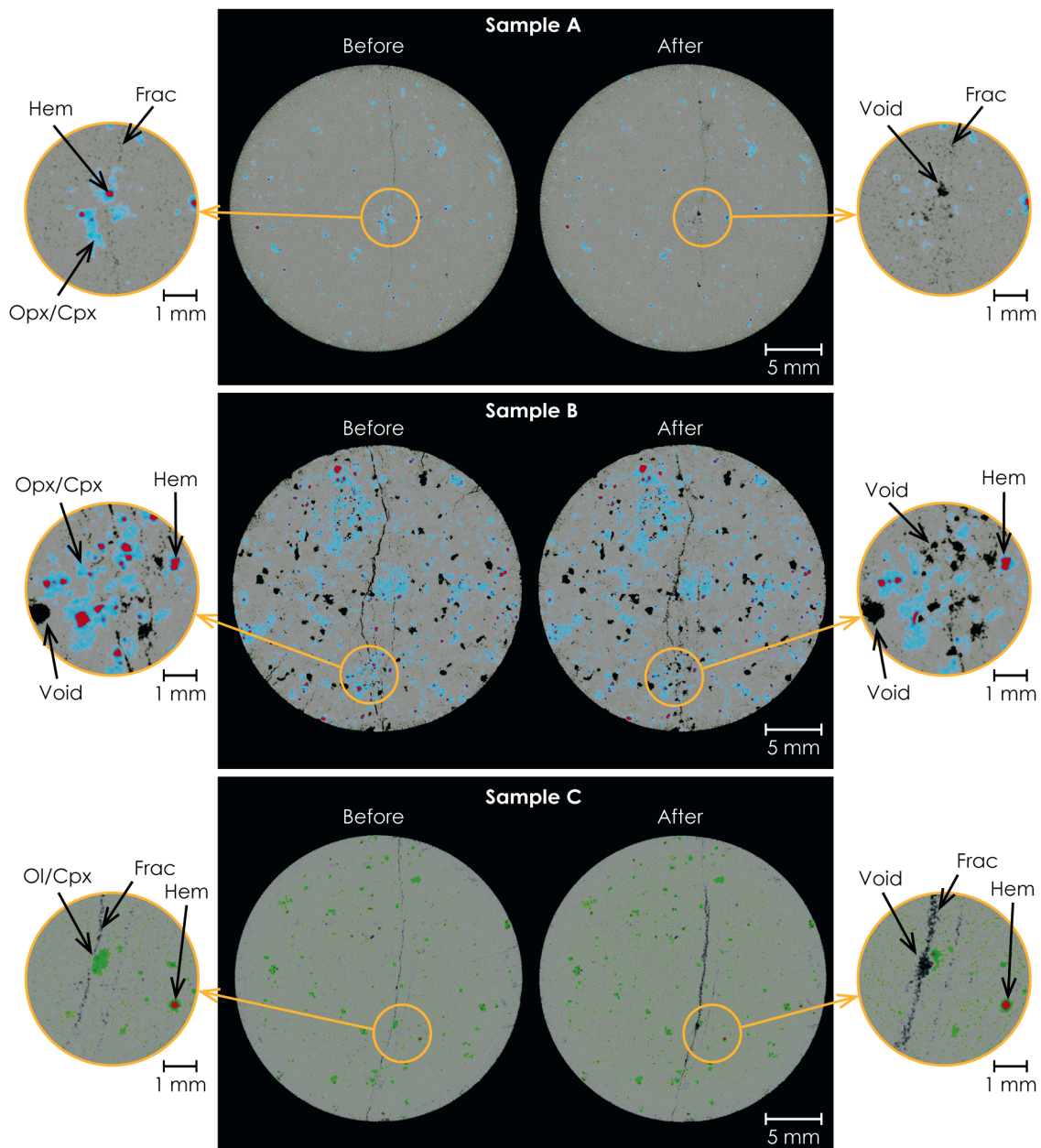


**Fig. 5.** X-ray CT slice images of the samples before and after the experiments, where Cpx, Opx, Hem, Ol, and Frac, respectively, denote clinopyroxene, orthopyroxene, hematite, olivine, and fracture.

clinopyroxene) were dissolved from the groundmass, while selective dissolution of phenocrysts of these minerals also led to void formation. It should be noted that selective dissolution of hematite was also observed in Sample C although it was less obvious due to the small amount and size of the mineral.

Fig. 6 compares the 3D distribution of voids in each sample, before and after the experiment, to confirm that sufficient void formation occurred in each sample to cause the substantial permeability enhancement. In the figure, continuous lines indicate the outline of the sample, while the dotted line approximates the fracture plane. Voids are colored according to their volumes. For Sample B, only voids within 5 mm of the fracture plane are shown, because this sample initially contained many voids throughout the entire body, which obscured the fracture plane.

All samples exhibited a substantial increase in the number of voids along the fracture plane, extending from the inlet to outlet of the sample. In Samples A and B, the distribution of voids is less continuous although

relatively small-volume voids are distributed over the entire fracture plane, reflecting the discrete distribution of Fe-rich phenocrysts (pyroxenes and hematite) in the samples. In contrast, Sample C exhibited a relatively continuous distribution of voids, resulting in a void with the largest volume of  $> 0.1 \text{ mm}^3$ , shown in purple. This purple void indicates the widening of the fracture aperture due to dissolution of fine-grained Fe-rich minerals (probably, clinopyroxene) in the groundmass. However, unlike the discrete distribution of smaller-volume voids, such large voids did not develop throughout the fracture plane. This may be because the confining pressure closed the larger voids that formed through uniform groundmass (fracture plane) dissolution. Indeed, the irregular decrease in differential pressure exhibited by Sample C (Fig. 3) indicates competing processes, i.e., both enhancing and reducing permeability.

As Sample C exhibited the smallest increase in permeability, despite forming the largest voids, we hypothesize that the dissolution of fine-grained minerals in groundmass is a less effective method of creating

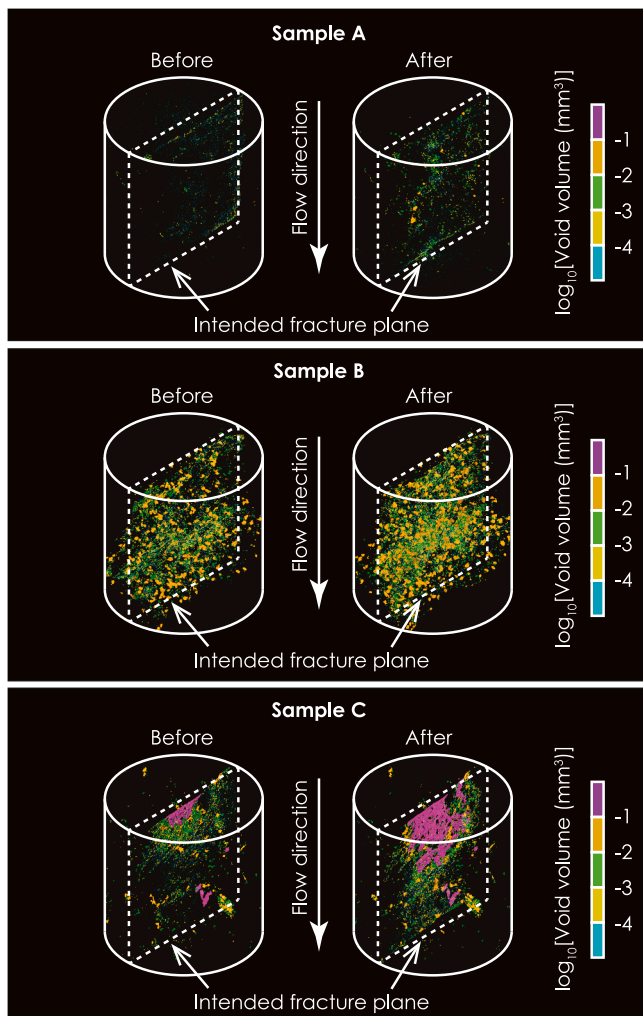


Fig. 6. 3-D distribution of voids in the samples before and after the experiments.

substantial permeability enhancement than the dissolution of phenocrysts. Therefore, the magnitude of permeability enhancement would be largely related to the void volume created by phenocryst dissolution. Moreover, the void volume would be largely determined by the areal percentage of phenocrysts (i.e., total area of phenocrysts exposed to the chelating agent solution).

### 3.3. Relationship between permeability enhancement and phenocryst dissolution

To examine the first hypothesis, the permeability enhancement factor was plotted against the total increase in void volume due to the selective dissolution of Fe-rich phenocrysts (pyroxenes, hematite and olivine) as shown in Fig. 7a. The purple voids with volumes of  $> 0.1 \text{ mm}^3$  (Fig. 6) were thus excluded when calculating the total increase in void volume. Moreover, to examine the second hypothesis, the total increase in void volume was plotted against the total areal percentage of Fe-rich phenocrysts, as shown in Fig. 7b. As expected, these plots verified that there is a clear linear relationship between the permeability enhancement factor and the total increase in void volume due to the selective dissolution of Fe-rich phenocrysts; similarly, there is a clear linear relationship between the total increase in void volume and the total areal percentage of Fe-rich phenocrysts.

We have shown that permeability enhancement could be achieved for three different types of volcanic rocks, through the selective

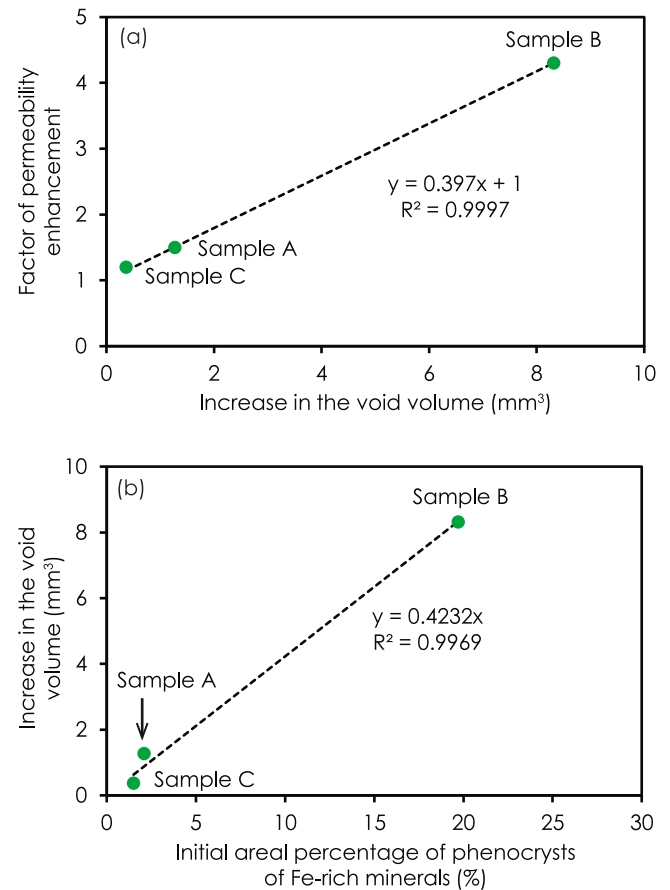


Fig. 7. Relationships between (a) the permeability enhancement factor and total increase in void volume due to dissolution of Fe-rich phenocrysts, and (b) between the total increase in void volume and total areal percentage of Fe-rich phenocrysts.

dissolution of Fe-rich phenocrysts leading to void formation. However, the volcanic rocks used in this study contained less than 20% phenocrysts in the areal percentage. Additionally, such grains were generally unevenly distributed within the rock samples. This implies that the formation of voids is only part of the permeability enhancement process, and the dissolution of non-Fe-rich phenocrysts and/or groundmass may also be involved. Additionally, the dissolution rates of minerals in volcanic rocks and glasses have different pH dependencies in water (Gudbrandsson et al., 2014; Rinder and von Hagke, 2021; Zhang et al., 2019), and mineral dissolution can be enhanced by the combining the effects of protons and chelating agents (Fredd and Fogler, 1998). Therefore, permeability enhancement may depend on pH conditions, with better permeability enhancement likely resulting from pH values other than 4. Therefore, future studies should investigate a process and optimum pH for enhancing permeability using chelating agents. Such research would strengthen the applicability and effectiveness of the chelating-agent-based chemical stimulation method and extend the use of EGSS worldwide.

## 4. Conclusions

The recently proposed method of chemically stimulating geothermal reservoirs using environment-friendly chelating agents to selectively dissolve minerals is considered a promising method that is complementary to hydraulic stimulation and provides a reasonable balance between the conflicting concerns of insufficient permeability enhancement and induced seismicity resulting from hydraulic stimulation in granitic reservoirs. To examine the applicability of chemical stimulation

to different types of reservoirs, we conducted chelating agent flooding experiments on fractured non-crystalline volcanic rock samples (i.e., dacitic, andesitic, and basaltic rocks) obtained from the Ahuachapán and Berlín geothermal fields in El Salvador.

The stimulation experiments were conducted on the fractured samples at 200 °C under confining pressure, with a 20 wt% aqueous solution of the readily biodegradable chelating agent, GLDA, at a pH of 4. The results demonstrated that the permeability of fractured volcanic rocks can be rapidly and substantially improved, by as much as four times within two hours. The increase in permeability is achieved by the selective dissolution of Fe-rich mineral phenocrysts (e.g., pyroxenes, olivine, and hematite), which creates stress-resistant voids. Moreover, the degree of permeability enhancement mainly depends on the amount of void volume that is created, and thus on the initial amount of phenocrysts that can be selectively dissolved.

This study extended the applicability of the chelating-agent-based chemical stimulation method to geothermal reservoirs in volcanic rocks. However, the process by which permeability is enhanced by void formation due to the dissolution of discretely distributed phenocrysts is not thoroughly understood yet, and different pH levels (other than 4) could result in a larger permeability enhancement. Therefore, further extensive studies on chelating-agent-based chemical stimulation are required to improve the reliability and efficacy of this new stimulation method and to achieve extensive use of EGSs in the future.

#### CRedit authorship contribution statement

**Luis Salalá:** Conceptualization, Methodology, Formal analysis, Investigation, Data curation, Writing – original draft, Visualization.  
**Ryota Takahashi:** Conceptualization, Methodology, Writing – review & editing.  
**Jonathan Argueta:** Validation, Writing – review & editing.  
**Jiajie Wang:** Validation, Writing – review & editing, Funding acquisition.  
**Noriaki Watanabe:** Conceptualization, Methodology, Data curation, Writing – original draft, Supervision, Project administration, Funding acquisition.  
**Noriyoshi Tsuchiya:** Validation, Resources, Writing – review & editing, Supervision, Project administration, Funding acquisition.

#### Declaration of Competing Interest

Noriaki Watanabe reports financial support was provided by Japan Society for the Promotion of Science. Jiajie Wang reports financial support was provided by Japan Society for the Promotion of Science. Noriyoshi Tsuchiya reports financial support was provided by Science and Technology Research Partnership for Sustainable Development. Jiajie Wang reports financial support was provided by Sumitomo Foundation. Noriaki Watanabe has patent pending to Japan Patent Office.

#### Data Availability

Data will be made available on request.

#### Acknowledgments

We would like to thank Miss. Kaori Takahashi at the Graduate School of Environmental Studies, Tohoku University, for assistance in conducting the chelating agent flooding experiments. We would also like to thank Dr. Shinichi Yamasaki at the Graduate School of Environmental Studies, Tohoku University, for assistance during ICP-OES analyses.

#### Funding

This study was partially supported by the Japan Society for the Promotion of Science (JSPS) through Grants-in-Aid for Scientific

Research (B) (no. 22H02015), Challenging Research (Pioneering) (no. 21K18200), Early-Career Scientists (no. 21K14571), and Scientific Research (S) (no. 22H04932). This study was also supported by the Japan Science and Technology Agency (JST) and the Japan International Cooperation Agency (JICA) through JST/JICA Science and Technology Research Partnership for Sustainable Development (SATREPS) program (no. JPMJSA1703) and by the Sumitomo Foundation through the Grant for Environmental Research Projects (no. 203137).

#### References

- Blender Online Community, 2018. Blender - a 3D Modelling and Rendering Package. Stichting Blender Foundation, Amsterdam. Available at: <http://www.blender.org>.
- Breede, K., Dzebisashvili, K., Liu, X., Falcone, G., 2013. A systematic review of enhanced (or engineered) geothermal systems: past, present and future. *Geotherm. Energy* 1, 4. <https://doi.org/10.1186/2195-9706-1-4>.
- Cladouhos, T.T., Petty, S., Swyer, M.W., Uddenberg, M.E., Grasso, K., Nordin, Y., 2016. Results from newberry volcano EGS demonstration, 2010–2014. *Geothermics* 63, 44–61. <https://doi.org/10.1016/j.geothermics.2015.08.009>.
- Deichmann, N., Giardini, D., 2009. Earthquakes induced by the stimulation of an enhanced geothermal system below Basel (Switzerland). *Seismol. Res. Lett.* 80, 784–798. <https://doi.org/10.1785/gssrl.80.5.784>.
- Farquharson, J.I., Kushnir, A.R.L., Wild, B., Baud, P., 2020. Physical property evolution of granite during experimental chemical stimulation. *Geotherm. Energy* 8, 14. <https://doi.org/10.1186/s40517-020-00168-7>.
- Fredd, C.N., Fogler, H.S., 1998. The influence of chelating agents on the kinetics of calcite dissolution. *J. Colloid Interface Sci.* 204, 187–197. <https://doi.org/10.1006/jcis.1998.5535>.
- Grigoli, F., Cesca, S., Rinaldi, A.P., Manconi, A., López-Comino, J.A., Clinton, J.F., Westaway, R., Cauzzi, C., Dahm, T., Wiemer, S., 2018. The November 2017 Mw 5.5 Pohang earthquake: a possible case of induced seismicity in South Korea. *Science* 360, 1003–1006. <https://doi.org/10.1126/science.aat2010>.
- Gudbrandsson, S., Wolff-Boenisch, D., Gislason, S.R., Oelkers, E.H., 2014. Experimental determination of plagioclase dissolution rates as a function of its composition and pH at 22°C. *Geochim. Cosmochim. Acta* 139, 154–172. <https://doi.org/10.1016/j.gca.2014.04.028>.
- Ishibashi, T., Watanabe, N., Asanuma, H., Tsuchiya, N., 2016. Linking microearthquakes to fracture permeability change: the role of surface roughness. *Geophys. Res. Lett.* 43, 7486–7493. <https://doi.org/10.1002/2016GL069478>.
- Ishibashi, T., Watanabe, N., Hirano, N., Okamoto, A., Tsuchiya, N., 2015. Beyond-laboratory-scale prediction for channeling flows through subsurface rock fractures with heterogeneous aperture distributions revealed by laboratory evaluation. *J. Geophys. Res. Solid Earth* 120, 106–124. <https://doi.org/10.1002/2014JB011555>.
- Kim, K.H., Ree, J.H., Kim, Y., Kim, S., Kang, S.Y., Seo, W., 2018a. Assessing whether the 2017 MW 5.4 Pohang earthquake in South Korea was an induced event. *Science* 360, 1007–1009. <https://doi.org/10.1126/science.aat6081>.
- Kim, K.I., Min, K.B., Kim, K.Y., Choi, J.W., Yoon, K.S., Yoon, W.S., Yoon, B., Lee, T.J., Song, Y., 2018b. Protocol for induced microseismicity in the first enhanced geothermal systems project in Pohang, Korea. *Renew. Sustain. Energy Rev.* 91, 1182–1191. <https://doi.org/10.1016/j.rser.2018.04.062>.
- Kwiatk, G., Saarno, T., Ader, T., Bluemle, F., Bohnhoff, M., Chendorain, M., Dresen, G., Heikkinen, P., Kukkonen, I., Leary, P., Leonhardt, M., Malin, P., Martínez-Garzón, P., Passmore, K., Passmore, P., Valenzuela, S., Wollin, C., 2019. Controlling fluid-induced seismicity during a 6.1-km-deep geothermal stimulation in Finland. *Sci. Adv.* 5, eaav7224. <https://doi.org/10.1126/sciadv.aav7224>.
- Lucas, Y., Ngo, V.V., Clément, A., Fritz, B., Schäfer, G., 2020. Modelling acid stimulation in the enhanced geothermal system of Soultz-sous-Forêts (Alsace, France). *Geothermics* 85, 101772. <https://doi.org/10.1016/j.geothermics.2019.101772>.
- Luo, J., Zhu, Y.Q., Guo, Q.H., Tan, L., Zhuang, Y.Q., Liu, M.L., Zhang, C.H., Zhu, M.C., Xiang, W., 2018. Chemical stimulation on the hydraulic properties of artificially fractured granite for enhanced geothermal system. *Energy* 142, 754–764. <https://doi.org/10.1016/j.energy.2017.10.086>.
- Mahmoud, M., Elkhatatny, S., AbdElgawad, K.Z., 2017. Using high- and low-salinity seawater injection to maintain the oil reservoir pressure without damage. *J. Pet. Explor. Prod. Technol.* 7, 589–596.
- Massachusetts Institute of Technology, 2006. The Future of Geothermal Energy: Impact of Enhanced Geothermal Systems (EGS) on the United States in the 21st Century. [https://www1.eere.energy.gov/geothermal/egs\\_technology.html](https://www1.eere.energy.gov/geothermal/egs_technology.html) and <https://geothermal.inel.gov> (Accessed 25 Apr, 2022).
- McClure, M.W., Horne, R.N., 2014. An investigation of stimulation mechanisms in Enhanced Geothermal Systems. *Int. J. Rock Mech. Min. Sci.* 72, 242–260. <https://doi.org/10.1016/j.ijrmms.2014.07.011>.
- Nemoto, K., Watanabe, N., Hirano, N., Tsuchiya, N., 2009. Direct measurement of contact area and stress dependence of anisotropic flow through rock fracture with heterogeneous aperture distribution. *Earth Planet. Sci. Lett.* 281, 81–87. <https://doi.org/10.1016/j.epsl.2009.02.005>.
- Park, S., Xie, L., Kim, K.I., Kwon, S., Min, K.B., Choi, J., Yoon, W.S., Song, Y., 2017. First hydraulic stimulation in fractured geothermal reservoir in Pohang PX-2 well. *Procedia Eng.* 191, 829–837. <https://doi.org/10.1016/j.proeng.2017.05.250>.

- Pinto, I.S.S., Neto, I.F.F., Soares, H.M.V.M., 2014. Biodegradable chelating agents for industrial, domestic, and agricultural applications—a review. *Environ. Sci. Pollut. Res. Int.* 21, 11893–11906. <https://doi.org/10.1007/s11356-014-2592-6>.
- Portier, S., Vuataz, F.D., Nami, P., Sanjuan, B., Gérard, A., 2009. Chemical stimulation techniques for geothermal wells: experiments on the three-well EGS system at Soultz-sous-Forêts, France. *Geothermics* 38, 349–359. <https://doi.org/10.1016/j.geothermics.2009.07.001>.
- Rinder, T., von Hagke, C., 2021. The influence of particle size on the potential of enhanced basalt weathering for carbon dioxide removal - insights from a regional assessment. *J. Clean. Prod.* 315, 128178 <https://doi.org/10.1016/j.jclepro.2021.128178>.
- Siratovich, P.A., Sass, I., Homuth, S., Bjornsson, A., 2011. Thermal stimulation of geothermal reservoirs and laboratory investigation of thermally induced fractures. *Translator* 35, 1529–1535.
- Tanaka, G., Hou, X., Ma, X., Edgecombe, G.D., Strausfeld, N.J., 2013. Chelicerate neural ground pattern in a Cambrian great appendage arthropod. *Nature* 502, 364–367. <https://doi.org/10.1038/nature12520>.
- Wang, J., Watanabe, N., Inomoto, K., Kamitakahara, M., Nakamura, K., Komai, T., Tsuchiya, N., 2021. Enhancement of aragonite mineralization with a chelating agent for CO<sub>2</sub> storage and utilization at low to moderate temperatures. *Sci. Rep.* 11, 13956. <https://doi.org/10.1038/s41598-021-93550-9>.
- Wang, J., Watanabe, N., Inomoto, K., Kamitakahara, M., Nakamura, K., Komai, T., Tsuchiya, N., 2022. Sustainable process for enhanced CO<sub>2</sub> mineralization of calcium silicates using a recyclable chelating agent under alkaline conditions. *J. Environ. Chem. Eng.* 10, 107055 <https://doi.org/10.1016/j.jece.2021.107055>.
- Watanabe, N., Hirano, N., Tsuchiya, N., 2008. Determination of aperture structure and fluid flow in a rock fracture by high-resolution numerical modeling on the basis of a flow-through experiment under confining pressure. *Water Resour. Res.* 44, W06412. <https://doi.org/10.1029/2006WR005411>.
- Watanabe, N., Hirano, N., Tsuchiya, N., 2009. Diversity of channeling flow in heterogeneous aperture distribution inferred from integrated experimental-numerical analysis on flow through shear fracture in granite. *J. Geophys. Res.* 114, B04208. <https://doi.org/10.1029/2008JB005959>.
- Watanabe, N., Takahashi, K., Takahashi, R., Nakamura, K., Kumano, Y., Akaku, K., Tamagawa, T., Komai, T., 2021. Novel chemical stimulation for geothermal reservoirs by chelating agent driven selective mineral dissolution in fractured rocks. *Sci. Rep.* 11, 19994. <https://doi.org/10.1038/s41598-021-99511-6>.
- Zang, A., Oye, V., Jousset, P., Deichmann, N., Gritto, R., McGarr, A., Majer, E., Bruhn, D., 2014. Analysis of induced seismicity in geothermal reservoirs – an overview. *Geothermics* 52, 6–21. <https://doi.org/10.1016/j.geothermics.2014.06.005>.
- Zhang, Y., Rimstidt, D.J., Huang, Y., Zhu, C., 2019. Kyanite far from equilibrium dissolution rate at 0–22°C and pH of 3.5–7.5. *Acta Geochim.* 38, 472–480. <https://doi.org/10.1007/s11631-019-00347-9>.